Complex conductivity reconstruction in multiple frequency electrical impedance tomography for fabric based pressure sensor

CL Yang[1], A Muhammad[1], Y Mohamadou[2], T I Oh[2], M Soleimani[1]

[1]Engineering Tomography Laboratory (ETL), Department of Electronic and Electrical Engineering, University of Bath, UK

[2]Department of Biomedical Engineering and Impedance Imaging Research Centre (IIRC), Kyung Hee University, Korea

Abstract-Fabric based electrical impedance tomography (EIT) pressure sensors aim to provide a pressure mapping image using current carrying and voltage sensing electrodes attached on the boundary of the fabric patch. This is potentially a very cost effective pressure mapping imaging solution in particular for imaging a large area. Recently, promising results are being achieved in resistivity imaging for these sensors. However, the fabric structure presents capacitive behaviour that could also be exploited for pressure mapping imaging. Complex conductivity reconstructions with multiple frequencies are implemented to observe both conductivity and permittivity changes due to the pressure applied on the fabric based sensor. The related mathematical frame work of complex conductivity reconstruction is presented. Experimental studies on detecting the change of complex conductivity using both an EIT tank phantom and a fabric based sensor are performed. First, electrical impedance spectroscopy on a fabric based sensor is performed. Secondly, the complex impedance tomography is carried out on fabric and on a traditional EIT tank phantom. Quantitative image quality measures are used to evaluate the performance of a fabric based sensor at various frequencies and against the tank phantom. The paper demonstrates for the first time the useful information on pressure mapping from the imaginary component of conductivity imaging.

Keyword: Pressure mapping imaging, EIT, fabric based sensor, complex conductivity reconstruction

1 Introduction

Electrical impedance tomography (EIT) is a fast and cost-effective technique for providing a tomographic conductivity image of a subject from boundary current-voltage data. EIT technique can be used as a fabric pressure mapping imaging solution (A Yao *at el*.,2012; R F Edlich *at el*., 2004; H Alirezaei *at el*., 2009; D S Tawil *at el*., 2011; K J Loh *at el*., 2009; A Yao *at el*., 2013; A Elsanadedy *at el*., 2012). Previous EIT imaging on fabric neglected the capacitive component of electrical impedance imaging, focusing only on pure resistivity changes. With pressure applied to a fabric patch whose boundary is clamped to maintain the fabric position, the conductivity of the proposed fabric changes with increasing pressure. Pressure induced shape changes over the sensor area make changes in conductivity distribution, the change in conductivity distribution leads to the change in current-voltage data in the EIT system. The EIT system displays the image of the conductivity changes from current-voltage data measured at the boundary of the fabric patch. Finally, the pressure distribution is estimated from the conductivity images.

Fabric based EIT has become a popular area of EIT study in recent years with various potential applications in mind. It can provide major improvements on the cost and operation complexity for clinical facilities as the technology is very cheap and simple. It can be applied to dynamic pressure seating systems and mattresses for patient's ulcer prevention (R F Edlich *at el*., 2004; M Reddy *at el*., 2006). Additionally, potential touch sensitive applications such as robotic skin are applicable and being developed (D S Tawil *at el*., 2011; W S Fulton *at el*., 1993). There are also different kinds of sensor structures which have been introduced and tested such as a rectangular fabric based sensor. Previous research has shown promising results on pressure detection (A Yao *at el*., 2013). The characteristic of conductive polymer for an EIT based sensor is evaluated in (A Elsanadedy *at el*., 2012) for analysing the non-linearity and hysteresis behaviour of the sensor. These could limit the application of pressure mapping imaging, in particular in dynamic situations with rapid changes of applied pressure. Further information through multiple frequency reconstruction and complex impedance imaging could potentially help to overcome these problems.

Most EIT experiments measure the resistivity information of the object, as the capacitive component is used in fewer applications. The resistive component can only provide information of the behaviour of the yarn. When the fabric patch has been stretched, the air gaps between yarns will change shape and this will be the capacitive information. If both resistance and capacitance are obtained, the reconstruction image of the fabric might become more accurate and reliable. By making a complex conductivity reconstruction one can obtain real and imaginary data for conductivity, where the permittivity change is mainly indicated by the imaginary part of voltage measurement and is highly related to the capacitive changes in the material. In order to validate this approach, this paper performs various experiments of complex conductivity reconstruction on both a saline phantom and a fabric based sensor, which provides a comparative study.

In this paper, an EIT-based fabric pressure sensor is presented and tested. In the proposed model, a pressure sensitive fabric patch is stretched over a deformable support along which electrodes are attached. In order to measure the pressure-induced shape change over the fabric patch, we inject a predetermined sequence of currents and measure the corresponding voltages through electrodes. Reconstructions are done by using complex impedance data. To identify how the imaginary part data changes with respect to frequency can benefit for the image reconstruction, a series of multiple frequency tests are employed. GREIT parameters are calculated to measure the image performance.

2 Complex impedance measurements on fabric

In order to analyse the impedance spectrum change of a piece of conductive fabric, a device was used to measure the complex impedance. The tetra-polar measurement method was used for characterizing of tested fabric material. Each electrode was made up of a pair of stainless steel bars. They immobilized the piece of tested fabric with sandwich structure and plastic bolts and nuts. The large surface and high conductive electrodes may minimize the effect of electrode contact impedance. Also, this is to ensure that injected current will flow uniformly across the fabric material to cancel out the geometric effect. Figure 1 shows the picture measuring impedance spectrum of a piece of fabric.

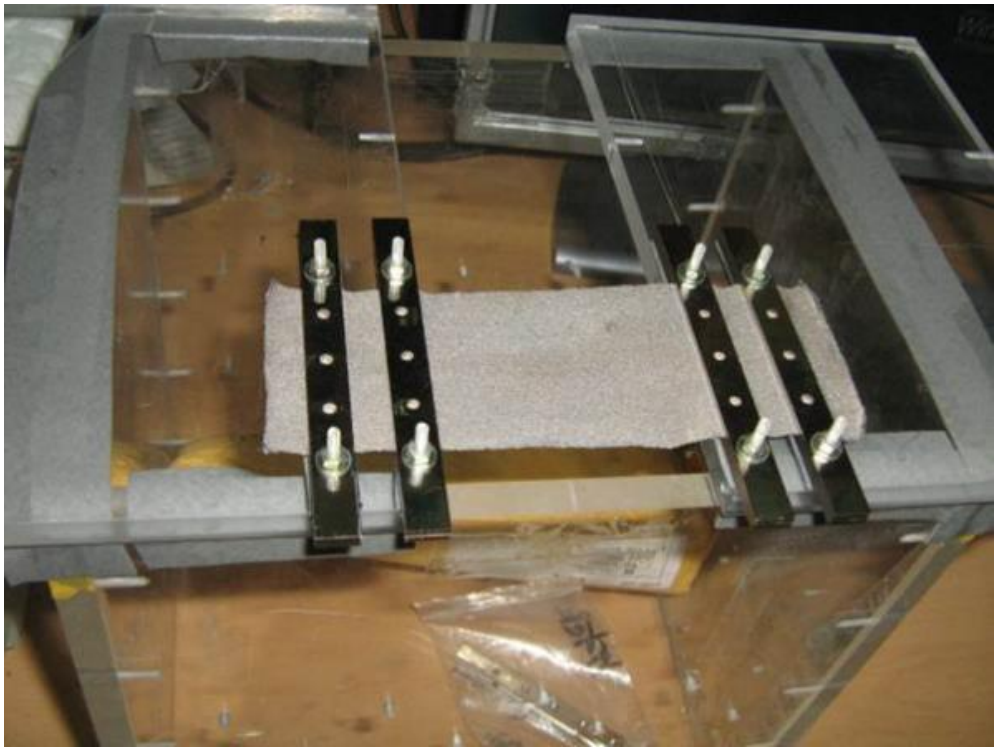

Figure 1 Picture of measuring impedance spectrum of a piece of fabric

Complex impedance values were measured with increasing pressure applied in a various frequency range. Figure 2 is generated by plotting the impedance values against different weight data. It can be observed that both real and imaginary parts of impedance measurement have variation between different frequencies. The impedance value increases as frequency increases.

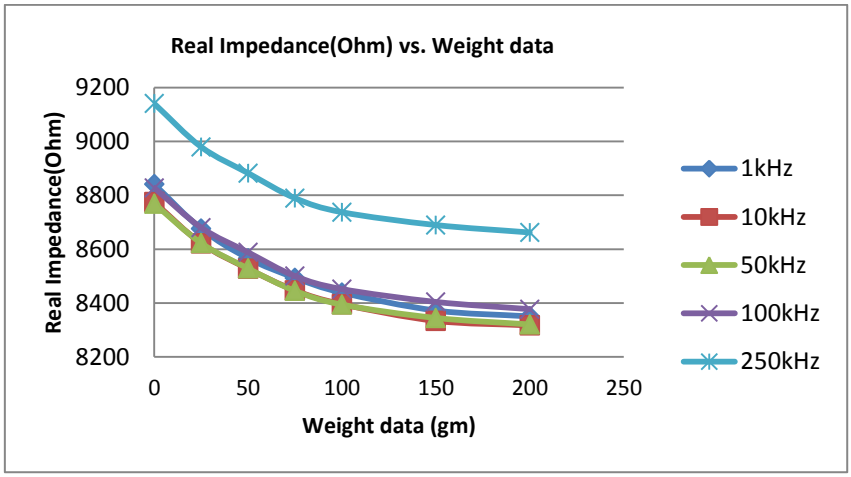

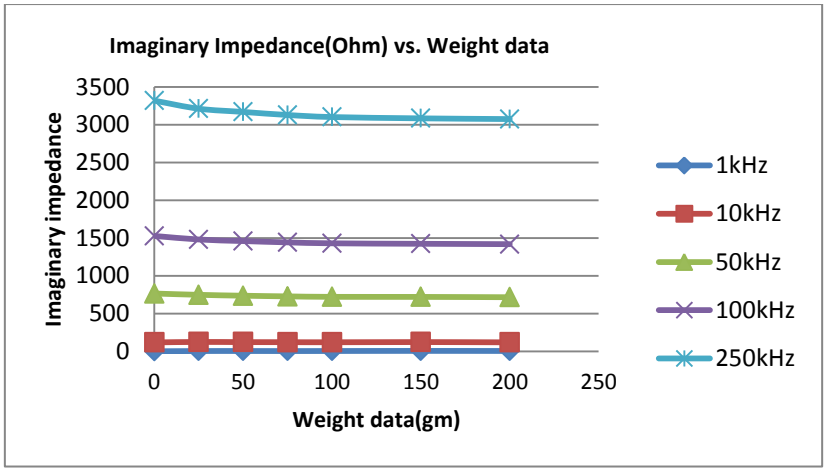

Figure 2 Plots of complex impedance value against weight data

There are measurable variations in real and imaginary parts of impedance of the fabric structure. This motivates complex impedance tomography for pressure sensing fabric. The mathematical modelling representing the impedance change as function of weights, is an electromechanical modelling, which is really beyond the scope of this paper.

3 Complex conductivity imaging

Let an imaging object occupy a two-dimensional region Ω with its boundary $\partial\Omega$. On the boundary, we attach electrodes e_l, $l=1,2,...,L$. A current with magnitude I and angular frequency ω is injected through a chosen pair of adjacent electrodes (e_l and e_{l+1}) to generate an electric potential, the resulting potential V is governed by

$$\nabla\cdot(\sigma^*\nabla V^*)=0 \qquad (1)$$

where $\sigma^* = \sigma + i\omega\varepsilon$ is the complex conductivity distribution. If σ and V_R are the real parts of admittivity and voltage respectively, while ε and V_I are the imaginary parts, the complex voltage measurements are formed by

$$\begin{aligned} J_{RR}\sigma + J_{RI}\varepsilon &= V_R \\ J_{IR}\sigma + J_{II}\varepsilon &= V_I \end{aligned} \qquad (2)$$

The Jacobian which corresponds to the effect of perturbations in conductivity on the real part of the measurements can be expressed as

$$J_{RR} = \frac{\partial V_R}{\partial \sigma} \qquad (3)$$

and the Jacobian corresponding to the effect of the conductivity perturbations on the imaginary part of the measurements is

$$J_{RI} = \frac{\partial V_I}{\partial \sigma} \qquad (4)$$

Therefore the remaining two combinations would be

$$J_{IR} = \frac{\partial V_I}{\partial \varepsilon} \quad (5)$$

and

$$J_{II} = \frac{\partial V_I}{\partial \varepsilon} \quad (6)$$

Thus the forward problem would become

$$J^* \partial \sigma^* = \partial V^* \quad (7)$$

$$\begin{bmatrix} J_{RR} & J_{RI} \\ J_{IR} & J_{II} \end{bmatrix} \begin{bmatrix} \sigma \\ \varepsilon \end{bmatrix} = \begin{bmatrix} V_R \\ V_I \end{bmatrix} \quad (8)$$

The complex conductivity perturbation $\partial\sigma^*$ in equation (7) can be computed by the linearized reconstruction algorithm via

$$\partial\sigma^* = (J^{*T} J^* + \lambda L)^{-1} J^{*T} \partial V^* \quad (9)$$

Where is J^* the Jacobian matrix for complex impedance, L is the regularization matrix, λ is the regularization parameter and V^* is the complex measured voltage.

4 EIT hardware

In order to measure the small changes of complex impedance due to the pressure, it requires high accurate EIT measurement system with uniform performance within the operating frequency range.

Experiments were carried out using the KHU Mark2 EIT system developed by the research group in Kyung Hee University Korea (K Y Kim *at el*., 2013; T I Oh *at el*., 2011). The KHU Mark2 EIT system consists of the following parts: (i) a PC with an USB port and EIT software, (ii) a main controller, DSP (TMS320LF2812A, Texas Instruments, USA) with an USB interface, (iii) an intra-network controller on a digital backplane, (iv) impedance measurement modules (IMM) and (v) switching circuits on an analogue backplane. Figure 3 and 4 show the device and its structure. The system can be operated from 50 Hz to 250 kHz. Output impedance of current source is over 1 MΩ at all chosen frequencies.

The main issue for obtaining the complex impedance spectrum in EIT hardware is maintaining the similar performance at the low and high operating frequency. The improved Howland current source with an injection current of 5 mA is adopted to maximize output impedance and wide-band voltage measurement amplifiers in IMM. Additionally, the circuit for calibrating the output impedance of current source is inserted at the operating frequency was over 1 MHz. Detailed description for EIT hardware is written in (K Y Kim *at el*., 2013; T I Oh *at el*., 2011).

Figure 3 Photo of the KHU Mark2

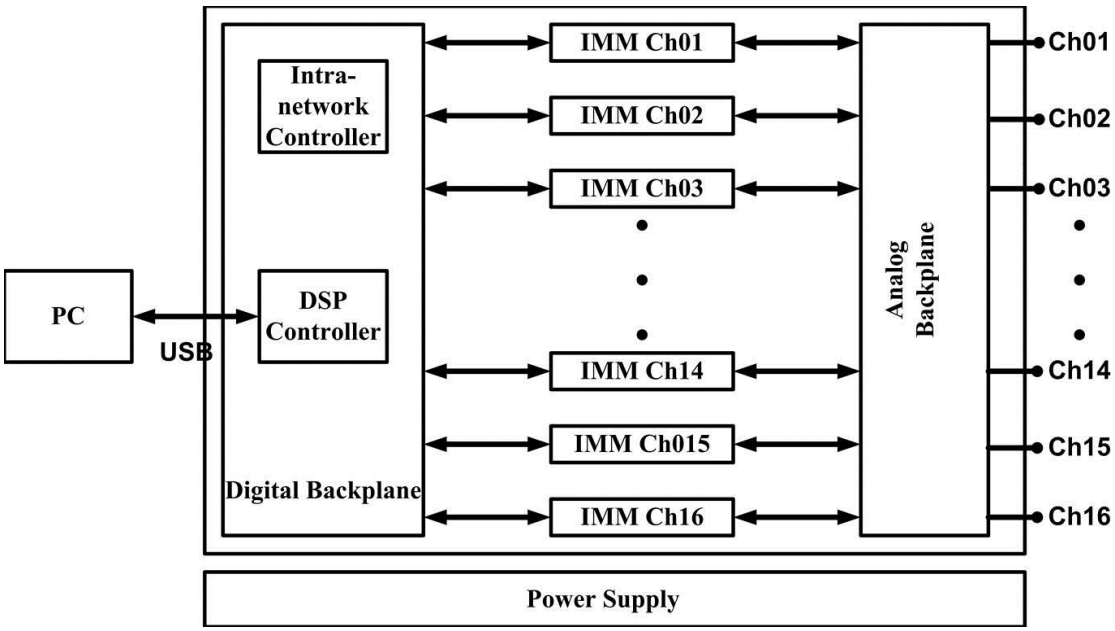

Figure 4 Structure of the KHU Mark2

It has high current amplitude stability of 0.009–0.095% and low total harmonic distortion of 0.2×10−3 to 0.08%. The signal to noise ratio is about 75-85 dB depending on frequencies and measurement channels.

By acquiring two different sets of voltage measurement data, the computer software is used to do a time difference image reconstruction. 16 electrodes EIT with adjacent

current pattern were used for multiple frequencies EIT imaging at 1 KHz, 10 KHz, 50 KHz, 100 KHz, and 250 KHz excitation frequencies.

5 Experimental validations

To evaluate the behaviour of complex conductivity changes due to the change of frequency, two types of sensor have been built: one is a typical 16 electrode tank phantom and the other is the 16 channel fabric based EIT sensor. The fabric based EIT sensor consists of a conductive fabric patch and a circular wooden frame with a sponge pad at the bottom. 16 narrow copper plates are used as boundary electrodes placed equidistant between the circular frame and the fabric. The conductive Fabric used here is developed by Eeonyx Corporation and named as EeonTex™ NW170-SL-PA-1500 with a surface resistivity of 1500 ohm/sq. +/- 15%. It is a microfiber nonwoven coated with a conductive formulation, generally used as dynamic pressure sensors (Eeonyx Corporation, 2009).

Conductivity distribution varies with the deformation of the fabric in respect with the pressure sensitive characteristic. Since the modal structure of the fabric-based sensor is not pure resistance, measurement of the imaginary part of conductivity distribution can be useful, particularly for the capacitive effect in the contact nodes and the change due to the deformation of the structure can provide valuable information. All experiments done in this paper include reconstruction images of both the real and imaginary parts of conductivity changes.

Two sets of experiments were carried out. Each of the tests included a tank phantom test and a fabric based sensor test. Reconstructions were using linear Tikhonov regularisation with regularisation parameter of 0.02. For adjacent current pattern EIT measurement, the centre position was considered to be the most difficult imaging position. Therefore the first test was to perform image reconstruction in the centre position for both sensors. Results are shown in figure 5.

Freq. (Hz)	Tank phantom (Real)	Tank phantom (Imaginary)	Fabric sensor (Real)	Fabric sensor (Imaginary)
	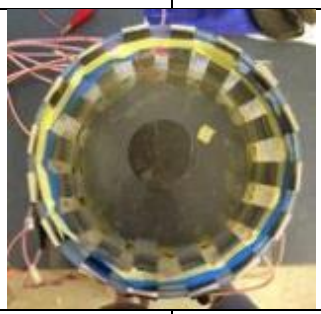		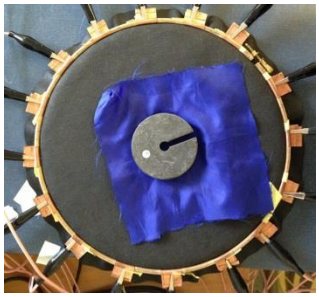	
5k	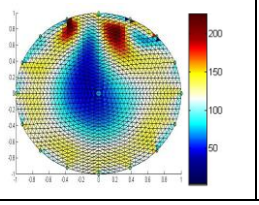	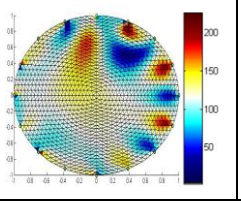	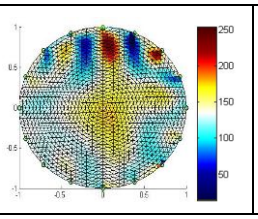	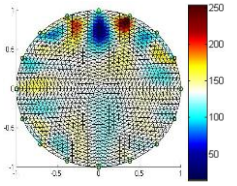

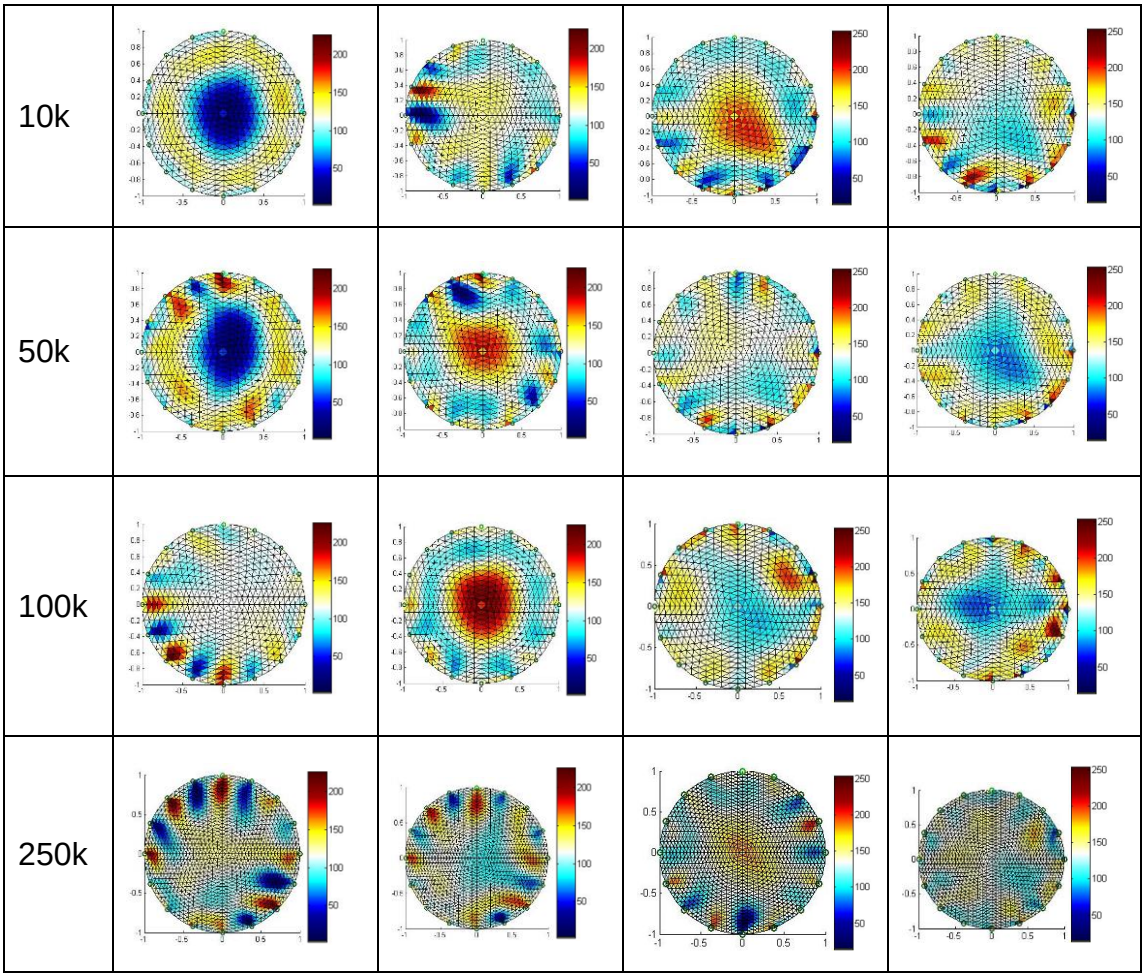

Figure 5 Complex conductivity reconstruction at a multiple frequency range with center pressure point (Test 1)

From figure 5, tank phantom results show better images than fabric sensor results as saline is much more conductive than the fabric material. Conductivity changes due to the insertion of the plastic rod is expected to be more significant than the conductivity changes due to pressure applied to the fabric.

Most typical EIT experiments only acquire real conductivity information which provides good image results like those in test 1 with a frequency of 10 kHz. As the frequency increases, it can be observed that image qualities of the real conductivity start to degrade while the imaginary part shows the opposite behaviour.

To further analyse the results, GREIT performance parameters (A Adler *at el*., 2009) have been used to perform image quality measurement. Figure 6 shows a set of figures of merit to characterize the image qualities based on GREIT. Based on images of point targets, several figures of merit are defined: amplitude response (AR), position error (PE), resolution (RES), shape deformation (SD) and ringing (RNG). AR measures the ratio of image pixel amplitudes in the target in the background to that in the reconstructed image. It is considered to be the most important figure of merit in quality measures. PE measures the extent to which reconstructed images faithfully represent the position of the image target. RES measures the size of reconstructed targets as a fraction of the medium.

Reconstruction algorithms typically create circular images for medium boundary. SD measures the fraction of the reconstructed one-fourth amplitude set which does not fit within a circle of the reconstructed area, this indicates shape changes of the

objects near the medium boundary. RNG indicates whether reconstructed images show areas of opposite sign surrounding the main reconstructed target area which is considered to be less important parameter.

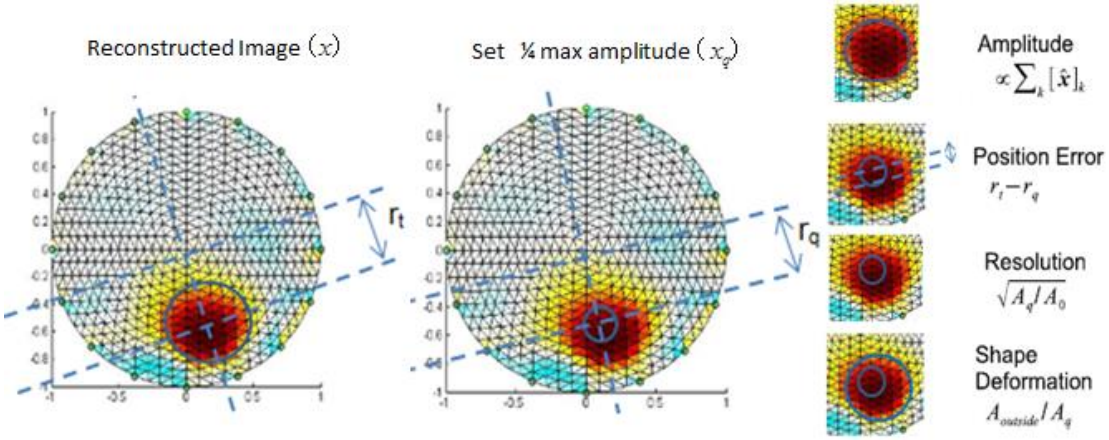

Figure 6 Performance figure of merit for evaluation of GREIT images

Change of GREIT parameters of tank phantom results with object at the centre with respect to frequency

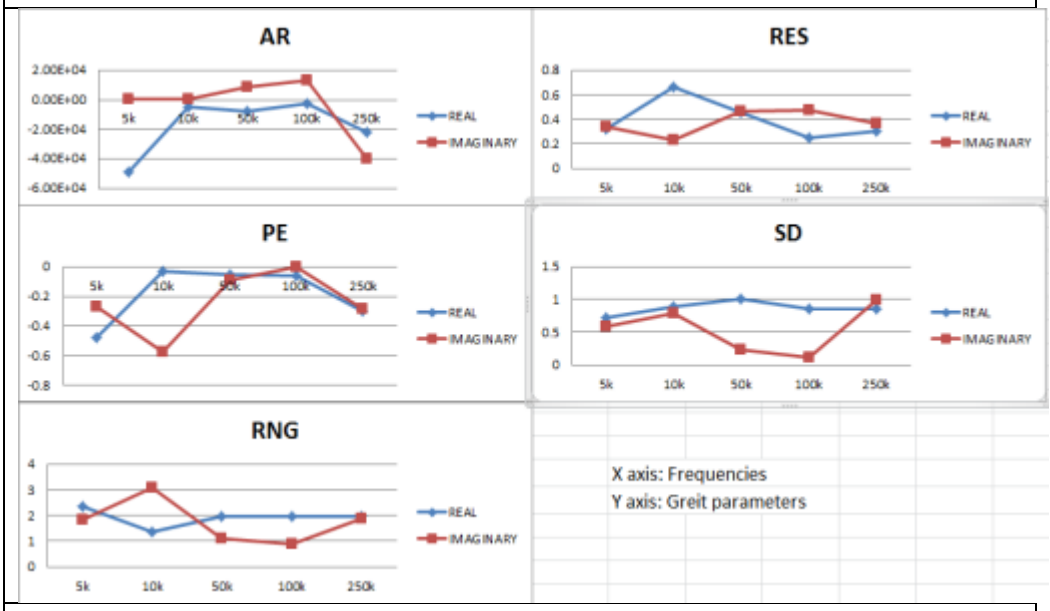

Change of GREIT parameters of fabric sensor results with object at the centre with respect to frequency

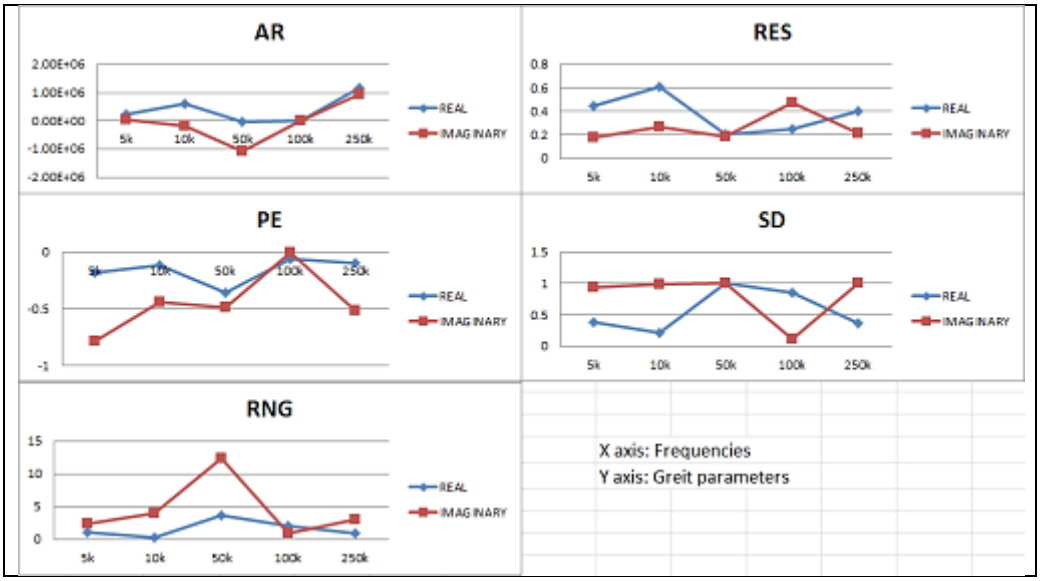

Figure 7 Evaluation of GREIT parameters AR, RES, PE, SD, and RNG as a function of point radial position (Test 1)

From figure 7, it can be observed that some important parameters such as RES and SD change relative to the quality of the reconstruction images. Focusing on the real part, it indicates RES drops with increasing SD for real conductivity reconstruction while frequency increases. For imaginary part data, it behaves in the opposite manner. It means that image from real part data is losing resolution and starting to get shape changing when frequency goes up. However imaginary part image is remaining shape and better resolution. PE behaves a bit randomly and shows small changes as the positions do not vary much from the centre. This shows that information from the imaginary part could be of benefit for reconstruction when the system is operated at high frequencies such 100k Hz. Performance of Imaginary images have bigger changes along the operating frequencies. Because same amount of capacitance variation can produce difference amount of change in the result at different operating frequencies.

The second test was to perform image reconstruction with the target position at one side for both sensors. Results are shown in figure 8.

Freq. (Hz)	Tank phantom (Real)	Tank phantom (Imaginary)	Fabric sensor (Real)	Fabric sensor (Imaginary)
	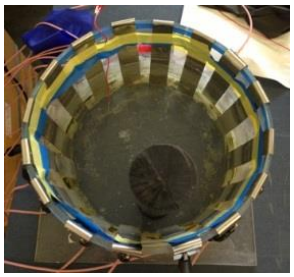		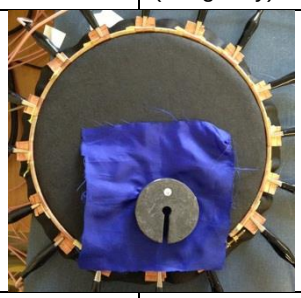	
5k	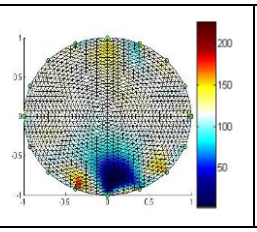	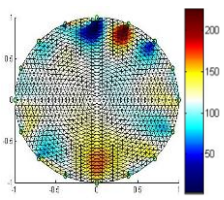	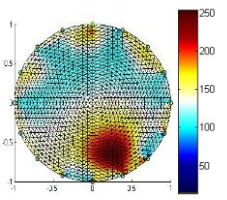	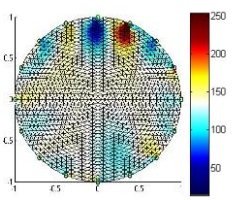

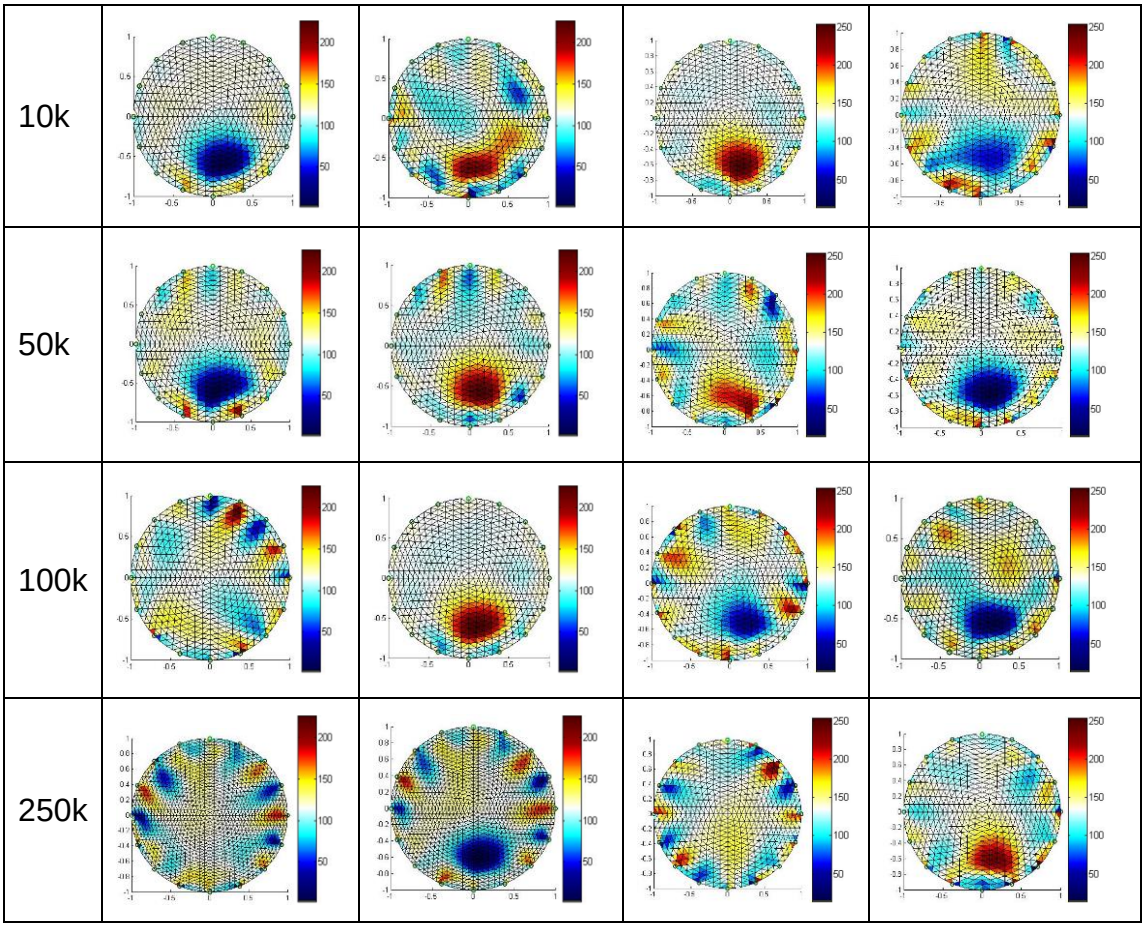

Figure 8 Complex conductivity reconstruction at a multiple frequency range with single pressure point by a side(Test 2)

Change of GREIT parameters of tank phantom results with object by a side with respect to frequency

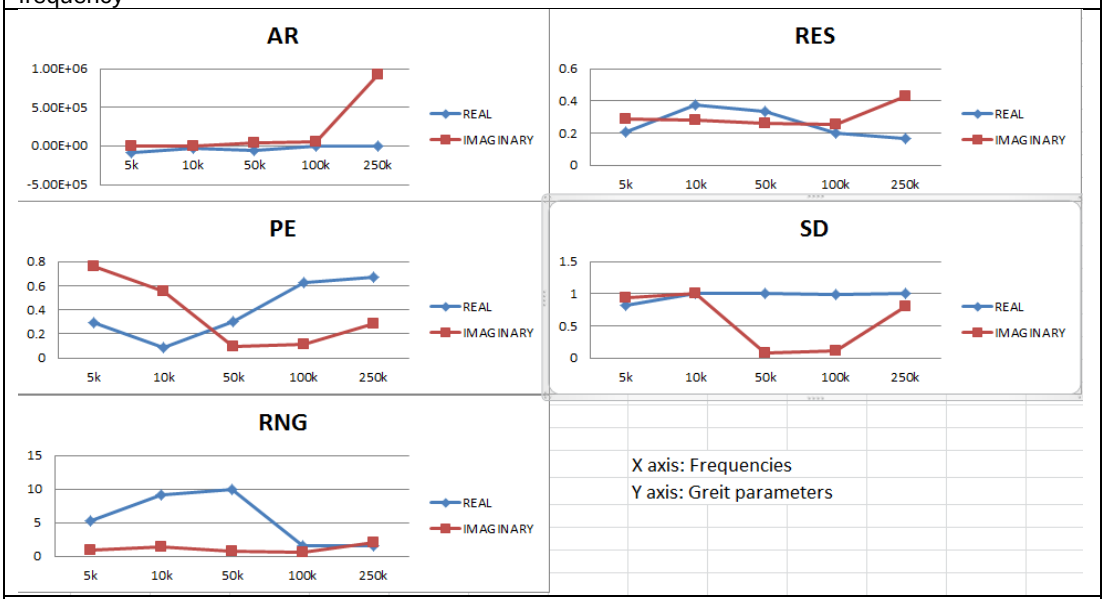

Change of GREIT parameters of fabric sensor results with object by a side with respect to frequency

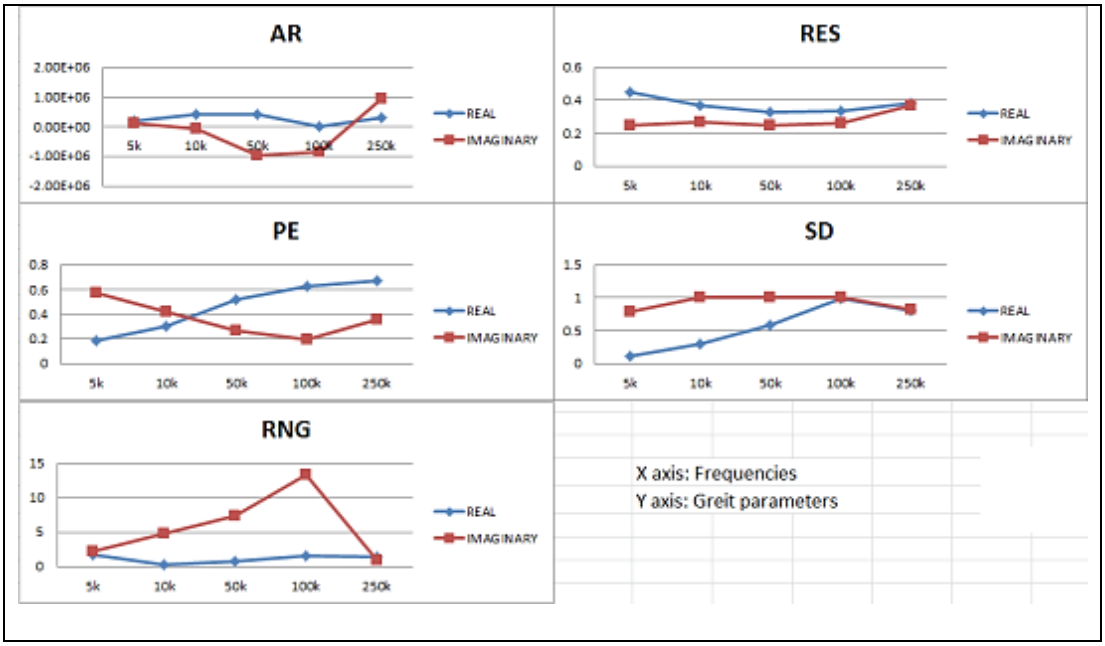

Figure 9 Evaluation of GREIT parameters AR, RES, PE, SD, and RNG as a function of point radial position (Test 2)

By observation from the images in figure 8, both the tank phantom and the fabric based EIT sensor have shown similar detectability for the object in different locations. Low distortion and apparent high quality of reconstruction images are produced in all situations. Conductivity distribution of the real part is always useful for typical low frequency EIT systems. However, the real part has failed to provide satisfactory image information at frequencies of 100 kHz and 250 kHz, while the imaginary part becomes more reliable with higher frequency.

Figure 9 shows the GREIT parameters in the second test. AR measures the image pixel amplitude therefore the value would be relied on the image scale. Both real and imaginary part data provide similar AR value except for one strange value appears in 250 kHz tank test may be due to systematic error. RES has obviously gone up for imaginary part image in tank phantom test. In fabric sensor experiment, real and imaginary part images have significant difference on SD at frequency 5 kHz. As frequency goes up, they both reach an SD value of about 0.8. It can be observed that PE for the real part data is increasing dramatically from around 0.2 to 0.6 in both tank and fabric test. To the contrary, PE for the Imaginary part decreases as operational frequency increases. These mean that at higher frequencies such as 100 kHz and 250 kHz, reconstructed images of imaginary part data locate more accurately refer to the actual object position.

6 Pressure mapping experiments with load and unload tests

In this paper a linear image reconstruction algorithm was used for time difference EIT imaging to recover complex impedance information. An electromechanical model needs to be developed to fully model a fabric based EIT sensor. Further work is needed to establish such forward and inverse modelling. To motive such a study in future here we investigate nonlinear behaviour of fabric through loading and unloading experiments. This experiment involved investigating the relationship between measured voltage and applied pressure. It was done by the application of

static loads at the side of the fabric. The load was continuously increased and later decreased. The load was initially made 1 kg, voltage readings were taken. It was then increased to 2kg on the same position, with the corresponding voltage measurements recorded. The procedure was repeated for 3 and 4 kg, and for the unloading procedure in steps of 3kg, 2kg up to 1 kg. The voltages measured were analysed to establish a pressure-voltage relationship.

The plots in figure 10 show the relationship between applied mass and the norm of the voltage difference between the loaded fabric and fabric background (in relaxed mode). The vertical axis gives the norm of the voltages differences, while the horizontal axis gives the applied mass. The norm of voltage differences are calculated separately for real and imaginary part of the measured voltage. The graphs are used to show the non-linearity in voltage norm for loading and unloading of the same mass. The norm of voltage differences provides a collective measure for nonlinearity of this electromechanically imaging problem. Figure 11 gives a summary of the reconstructed images due to loading and unloading of the fabric patch. Future work should focus on more sophisticated electromechanical modelling enabling reconstruction of nonlinear behaviour.

For the real part images between 5 kHz and 50 kHz, the loading voltage norm experiences a non-linear increase with an increase in mass. Consequently, the unloading phase experiences a similar relationship. However, with a slight drift in the norm voltage values between loading and unloading. These drift during unloading can be attributed to the loss in mechanical structure of the already loaded-fabric due to stretch.

Also, for the 10 kHz and 50 kHz excitation, the non-linearity exhibited by the real image is similar to that of the imaginary image. These frequencies present the best complex impedance results. After 50 kHz, the non-linearity in the real part image increases, with the 250 kHz frequency having an indescribable voltage-mass relationship for both loading and unloading. For the imaginary part images at 100 and 250 kHz, the bias between loading and unloading reduces and resembles that of real part image obtained at 10 and 50 kHz.

Generally, it was established that the offset between the norm voltage between loading and unloading is nearly the same for the real part images between 10 and 50 kHz, as well as for the imaginary part images between 100 and 250 kHz.

Freq. (kHz)	Conductivity image (Real) loading and unloading cycle	Permittivity image (Imaginary) loading and unloading cycle
5	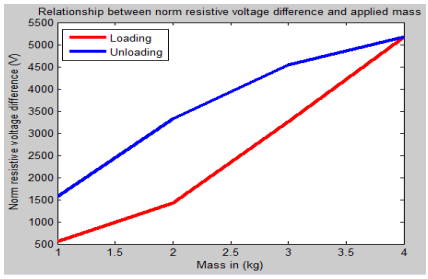	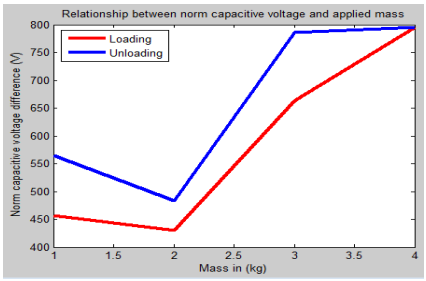
10	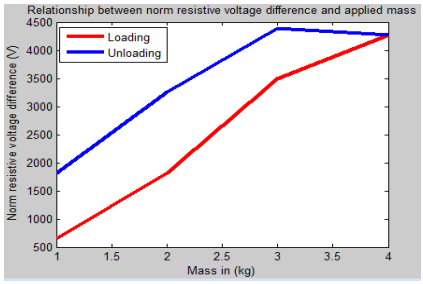	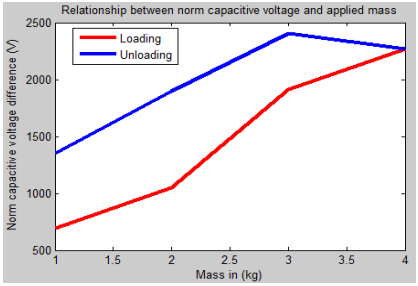
50	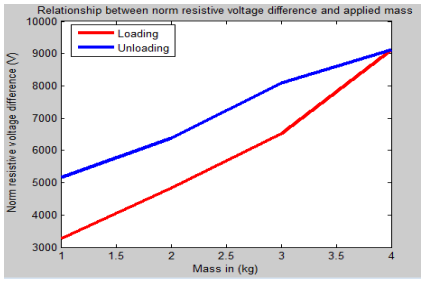	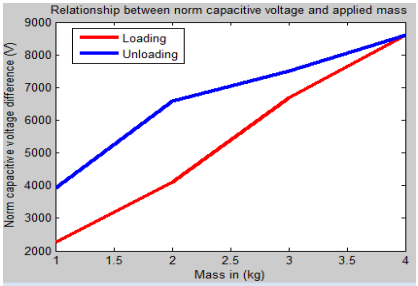
100	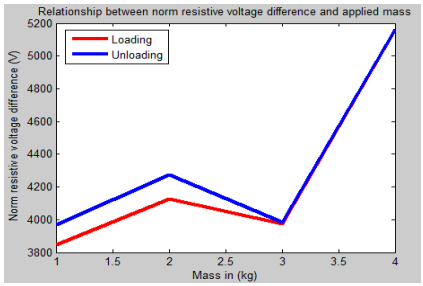	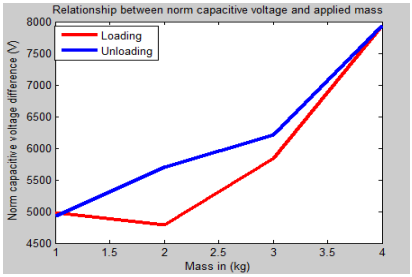
250	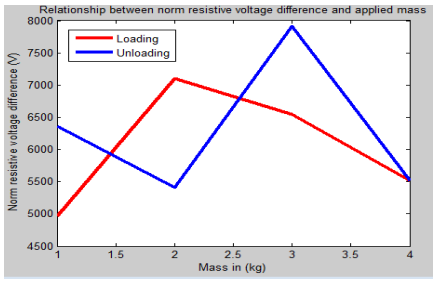	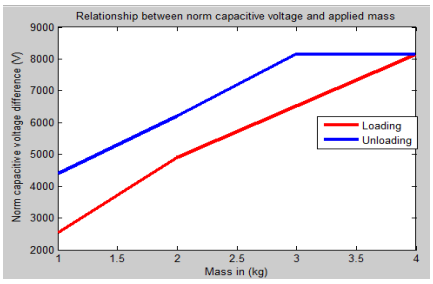

Figure 10: Norm of voltage differences between a relaxed fabric and loading and unloading voltage

Mass (kg)			1 kg	2 kg	3 kg	4 kg
Freq (kHz)						
5	Real	Load	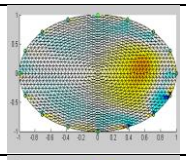	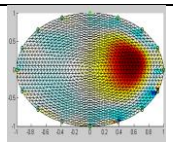	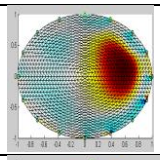	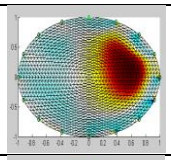
		Unload	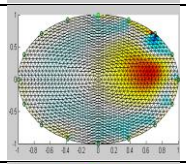	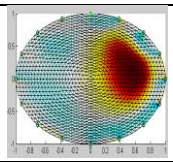	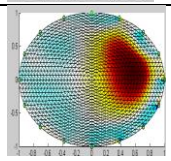	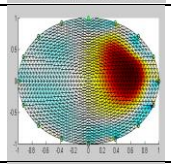
	Imaginary	Load	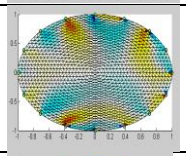	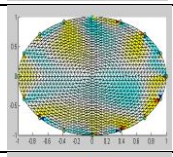	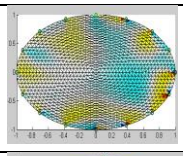	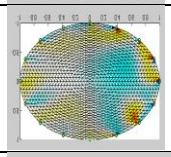
		Unload	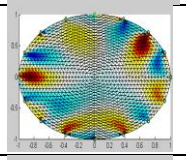	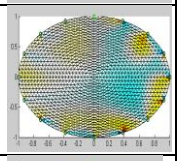	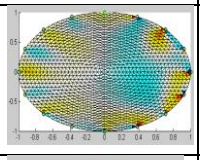	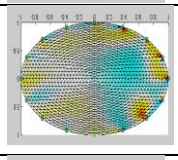
10	Real	Load	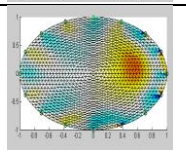	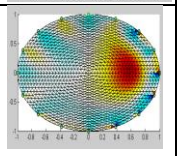	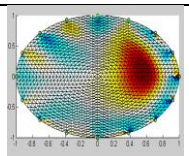	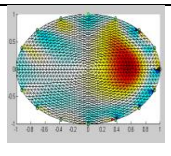
		Unload	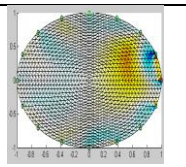	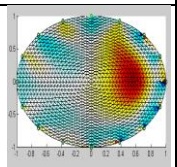	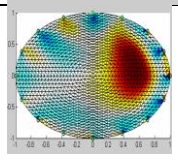	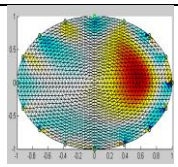
	Imaginary	Load	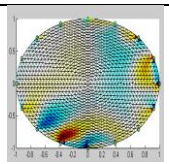	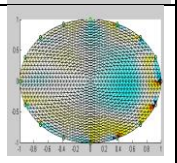	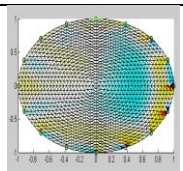	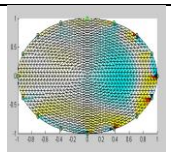
		Unload	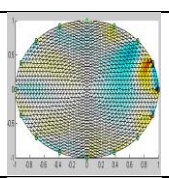	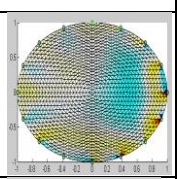	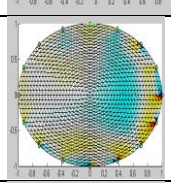	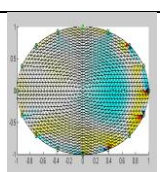
50	Real	Load	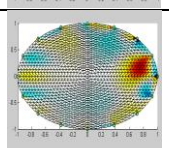	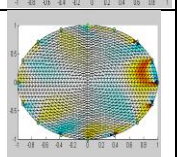	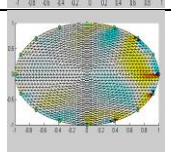	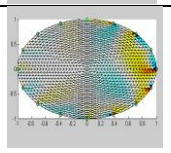
		Unload				

	Imaginary	**Load**	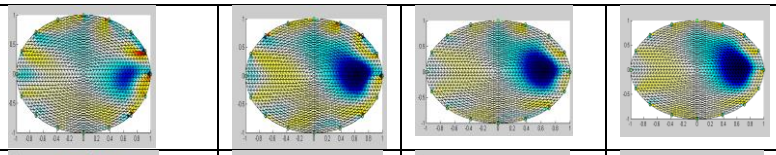			
		Unload	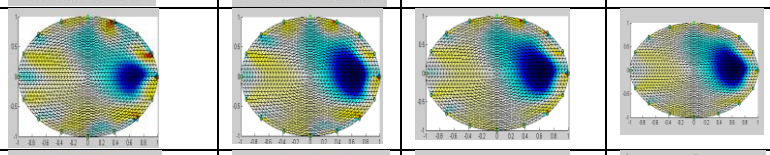			
100	**Real**	**Load**	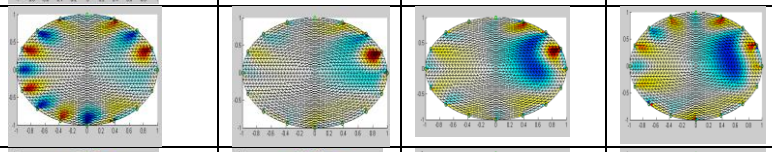			
		Unload	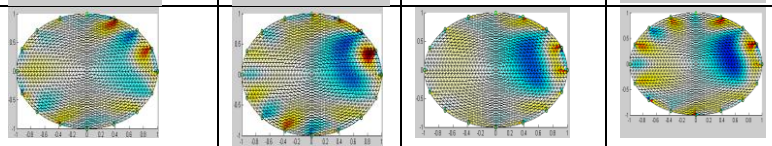			
	Imaginary	**Load**	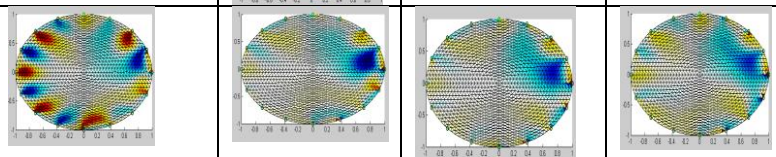			
		Unload	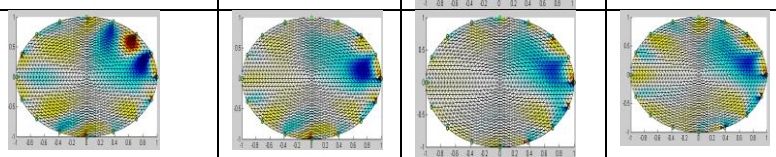			
250	**Real**	**Load**	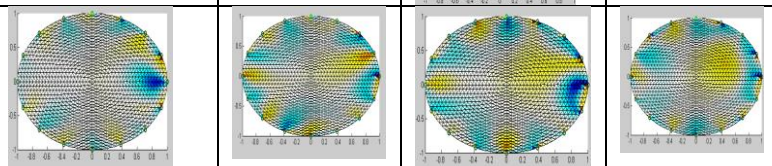			
		Unload	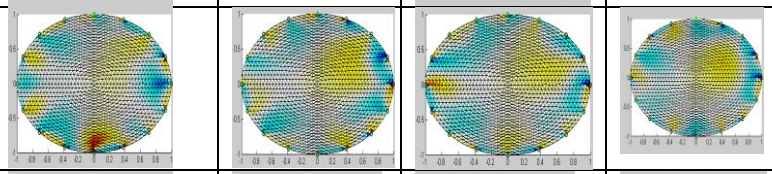			
	Imaginary	**Load**	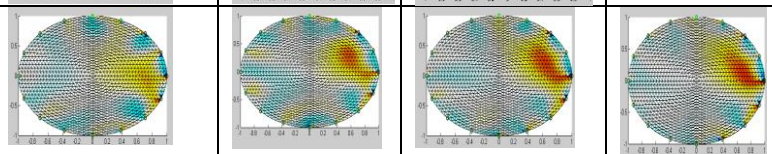			
		Unload	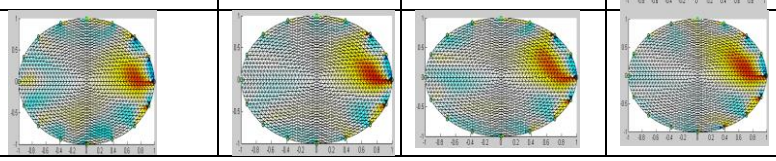			

Figure 11: Reconstructed real and imaginary part images for loading and unloading mode

7 Conclusions

The fabric structure exhibits both resistive and capacitive variations under mechanical loading conditions. For the first time in this paper images of capacitive changes due to pressure change were investigated. The imaginary part of conductivity changes become more reliable when higher frequency is applied to the fabric. This means that the capacitive components are useful when fabric sensor tests are performed at high frequencies. Measured voltages for real and imaginary parts are showing hysteresis behaviour, essentially motivating future studies of nonlinear electromechanical behaviour of the fabric based EIT. It is important to see that the results of the paper shows cases that real or imaginary may not produce satisfactory results and this is important when evaluating the repeatability and reliability of pressure mapping imaging using complex impedance tomography. The results of the paper are promising in terms of usefulness of the capacitive component of the complex impedance in the same way as the resistive component. Further investigation with more intensive frequency selections would potentially make improvement on evaluating better results. Therefore future studies will include optimising the hardware system performance. There will also be interest on doing spectral reconstruction, including direct reconstruction of cole-cole parameters, and frequency difference imaging. Further scientific work is needed to develop future applications of the pressure mapping EIT as a low cost alternative for pressure mapping imaging.

References

A Adler, J H Arnold, R Bayford, A Borsic, B Brown, P Dixon, T J C Faes, I Frerichs, H Gagnon, Y Gärber, B Grychtol, G Hahn, W R B Lionheart, A Malik, R P Patterson, J Stocks, A Tizzard, N Weiler, G K Wolf (2009),“GREIT: a unified approach to 2D linear EIT reconstruction of lung images, " Physiol Meas, Vol 30, No.6.

A Elsanadedy, Y Mamatjan, M Ahmadi, A Adler (2012),” Characterisation of Conductive Polymer for EIT based Sensor,” International Conference on Electrical and Computer Systems (ICECS'12), Ottawa, Canada.

A Yao, M Soleimani (2012),"A pressure mapping imaging device based on electrical impedance tomography of conductive fabrics", Sensor Review, Vol. 32, Iss: 4, pp.310 - 317.

A Yao, C L Yang, J K Seo, M Soleimani (2013),” EIT-based fabric pressure sensing,” Computational and mathematical methods in medicine, Vol 2013, Article ID 405325.

D S Tawil, D Rye, M Velonaki (2011),” Improved image reconstruction for an EIT based sensitive skin with multiple internal electrodes, ” IEEE Transactions on robotics, Vol. 27, No.3.

Eeonyx Corporation (2009),”NW170-SL-PA-1500, Eeontex Conductive Nonwoven Fabric”.

H Alirezaei, A Nagakubo, Y Kuniyoshi (2009),"A tactile distribution sensor which enables stable measurement under high and dynamic stretch", 2009 IEEE Symposium on 3D User Interfaces.

K J Loh, T C Hou, J P Lynch, N A Kotov (2009),” Carbon nanotube sensing skins for spatial strain and impact damage identification, ” Journal of non-destructive evaluation, Vol.28, pp 9-25.

K Y Kim, H Wi, P J Yoo, T I Oh, E J Woo (2013),“Performance Evaluation of KHU Mark2 Parallel Multi-frequency EIT system,” Journal of Physics, 224(2010)012013.

M Reddy, S S Gill, P A Rochon (2006),"Preventing pressure ulcers: A systematic review", JAMA: The journal of the American medical association, **296**(8): p. 974-984.

R F Edlich, K L Winters, C R Woodard, R M Buschbacher, W B Long, J H Gebhart, E K Ma (2004),“Pressure ulcer prevention,” Journal of Long-term Effects of Medical Implants, 14(4):285-304.

T I Oh, H Wi, D Y Kim, P J Yoo and E J Woo (2011),“ Fully parallel multi-frequency EIT system with flexible electrode configuration: KHU Mark2,” Physiol. Meas., Vol. 32, pp. 835-49.

W S Fulton, R T Lipczynski (1993),"Body-support pressure measurement using electrical impedance tomography", Engineering in Medicine and Biology Society, Proceedings of the 15th Annual International Conference of the IEEE.